DOI: 10.1002/anie.201201742

Graphite Nanoneedles

Edge-Plane-Rich Nitrogen-Doped Carbon Nanoneedles and Efficient Metal-Free Electrocatalysts**

*Rafael Silva, Jafar Al-Sharab, and Tewodros Asefa**

Carbon nanomaterials exhibit some unusual physical, chemical, and mechanical properties, such as light absorption, mechanical stiffness, and high conductivity,[1] owing to the unique geometric arrangement of the carbon atoms[2] and the extensive conjugated sp^2–sp^2 linkages and π-orbital electron delocalization in their structures.[3,4] These structural features also enable carbon nanomaterials to serve as robust electrocatalysts,[5] with their edge planes displaying the most electrocatalytic activity and with dopants, such as nitrogen further improving this activity.[6] However, the edge planes exist only in a small area in carbon nanomaterials, such as at the tips of carbon nanotubes or at defect sites on the basal planes of graphitic nanostructures.[7] Thus, this inherent low-density of edge planes in many carbon nanomaterials limits their electrocatalytic activities.[8] Herein we report novel cellulose-derived nitrogen-doped carbon nanoneedles (CNNs) with well-organized graphitic layers, and more importantly, large proportions of nitrogen-doped edge planes that display very high electrocatalytic activities. We also showed that these materials can serve as highly efficient metal-free catalysts and electrocatalysts for fuel cells. Although cellulose materials have been previously used to make carbon nanostructures,[9,10] the nanomaterials reported herein, that is, carbon nanoneedles have very different structures from these previously reported materials.

Our synthetic route to the novel CNNs relies on cellulose nanowhiskers (CeNWs).[11,12] In our synthetic approach, CeNWs are uniquely employed to serve both as a template as well as a carbon source for the graphitic nanoneedles. CeNWs are needle-shaped nanomaterials with high aspect ratios and very high crystallinity, with crystallinity values as high as 90% or more depending on the natural origin of the cellulose.[13] CeNWs can easily be obtained by kinetically controlled hydrolysis of natural cellulose under various conditions.[14] Furthermore, their surface charges can easily be controlled by changing the solutions used for the hydrolysis of bulk cellulose. For instance, negatively charged CeNWs can easily be synthesized by hydrolyzing bulk cellulose in concentrated acid solution.[15] The resulting CeNWs could serve as a template for deposition of electropositive substances and for making other nanostructured materials.

In the synthesis of CNNs, first needle-shaped CeNWs/metal-complex/silica core–shell–shell nanoreactors were synthesized using CeNWs as a template. This was achieved by dispersing negatively charged CeNWs in ethanol (Supporting Information, Figure S1), followed by assembling a positively charged layer of metal amine complex ions around the CeNWs (Scheme 1). Uniform silica shells were then coated around the metal amine coated CeNWs by a sol–gel process, which involved the hydrolysis and condensation of tetraethyl orthosilicate (TEOS). The CeNWs-supported metal amine complexes served two functions: 1) they helped with the deposition of negatively charged silicates, which later formed the silica shells around the CeNWs, and 2) they assisted with the subsequent graphitization process of CeNWs into CNNs by serving as catalysts.[16]

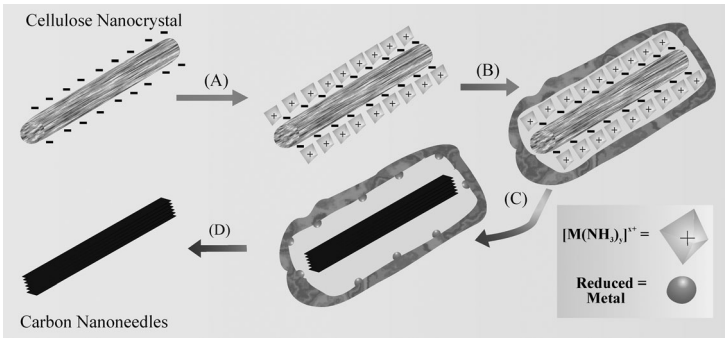

Scheme 1. Synthesis of CNNs. A) Surface modification of negatively charged CeNWs by metal amine complexes; B) Deposition of silica shells around CeNWs-supported metal complexes; C) Thermal treatments to convert the CeNWs in the core of CeNW/metal complex/silica core–shell–shell nanoneedles into graphite; and D) Removal of silica shells to produce free-standing CNNs.

The CeNWs/metal amine/silica core–shell–shell nanoneedles were then subjected to three sequential stages of high-

[*] R. Silva, Prof. Dr. T. Asefa
Department of Chemistry and Chemical Biology, Rutgers, The State University of New Jersey
610 Taylor Road, Piscataway, NJ 08854 (USA)
E-mail: tasefa@rci.rutgers.edu
Homepage: http://chem.rutgers.edu/asefa_teddy
Prof. Dr. T. Asefa
Department of Chemical and Biochemical Engineering, Rutgers, The State University of New Jersey
98 Brett Road, Piscataway, NJ 08854 (USA)
Dr. J. Al-Sharab
Department of Materials Science and Engineering, Rutgers, The State University of New Jersey
607 Taylor Road, Piscataway, NJ 08854 (USA)

[**] T.A. acknowledges the financial support of the US National Science Foundation (NSF) through CAREER Grant CHE-1004218, NSF DMR-0968937, NSF NanoEHS-1134289, NSF American Competitiveness and Innovation Fellowship (NSF-ACIF), and NSF Special Creativity grant. R.S. acknowledges the CAPES (Brazil) and the Fulbright Agency (USA) for their Fellowships for his graduate study.
Supporting information for this article is available on the WWW under http://dx.doi.org/10.1002/anie.201201742.

temperature treatment (Figure S2). In the first stage, a moderate temperature (100 °C) was used to assist with condensation of the silanol groups of the silica shells so that silica shells with low plasticity and porosity could form.[17] In the second stage, the material was treated at high enough temperatures (200 °C for 2 h, followed by 300 °C for 2 h) to let the CeNWs undergo dehydration (carbonization) without significant degradation of their carbon–carbon bonds. This thermal treatment led to the conversion of CeNWs into amorphous carbon. In the final stage, the material was annealed at 1200 °C to convert the amorphous carbon into graphitic carbon. During these processes, the silica shells around the CeNWs served as robust nanoreactors and kept the core–shell nanoneedles intact (as seen in Figure S2). Furthermore, the silica shells assisted the graphitization process by trapping any volatile carbon species and increasing the local pressure inside the cores of the core–shell–shell nanostructures. On the other hand, the trace metal ions, which were sandwiched between the CeNWs cores and silica shells of CeNWs/metal complex/silica core–shell–shell nanoneedles, functioned as nucleation centers for the growth of CNNs during the graphitization process. In the final step, the CNNs were extracted from the resulting CNN/silica core–shell nanoneedles by etching away the silica shells from the nanoneedles with aqueous NaOH solution (Scheme 1).

The transmission electron microscope (TEM) images of CNNs obtained with $[Pt(NH_3)_6]^{4+}/[Ru(NH_3)_6]^{3+}$ as the metal complexes (Figures 1a and b) show high aspect ratio nanoneedles having an average length of approximately 150 nm and an average width of around 17 nm (Figure 1e,f). Their high-resolution TEM (HRTEM) image (Figure 1c) depicts layered graphitic structures oriented along the elongated axis of the nanoneedles. This structure is corroborated by the selected-area electron diffraction (SAED) pattern (Figure 1d), which shows diffraction signals at 3.34, 2.04, 1.68, and 1.19 Å. As these signals correspond to the characteristic diffraction peaks of hexagonal crystalline structure of graphite,[18] the result suggests that the CNNs have highly organized graphitic layers.

The X-ray photoelectron spectroscopy (XPS) results for the CNNs obtained from the core–shell–shell nanoneedles with $[Pt(NH_3)_6]^{4+}/[Ru(NH_3)_6]^{3+}$ ions (Figure 2a, and Table S1) show non-detectable Ru, but a trace amount (0.5 wt %) of Pt. However, the TEM and HRTEM images do not reveal the presence of Pt nanoparticles in the samples, as is further confirmed by underpotential hydrogen adsorption measurement (Figure S9), which also ruled out the presence of Pt nanoparticles in the CNNs. Thus, when these results are combined, they strongly suggest that the observed trace amount of Pt in the XPS spectra must be due to some very small Pt species. This is indeed found to be the case when we closely look at the XPS spectrum. The binding energy for Pt 4f 7/2 peak appears at 71.6 eV, which is slightly shifted to higher energy compared to the typical bands in the range of 70.8–71.3 eV that Pt nanoparticles exhibit. According to Isomura et al., such a shift for the Pt 4f 7/2 peak is indicative of the presence of small Pt clusters composed of 7 to 15 atoms.[19]

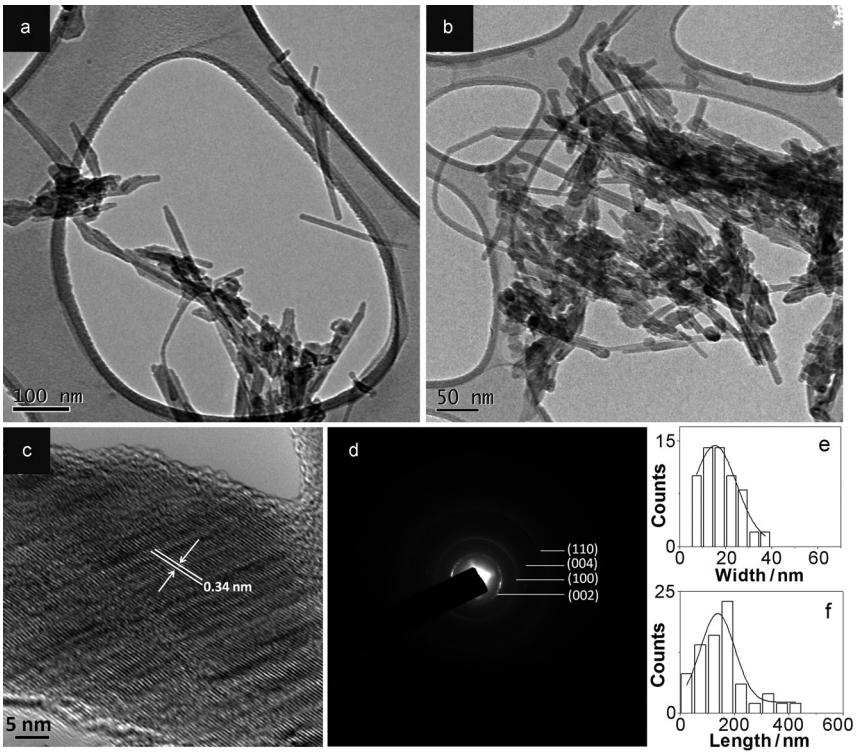

Figure 1. CNNs obtained from CeNW/$[Pt(NH_3)_6]^{4+}/[Ru(NH_3)_6]^{3+}$/silica: a) low magnification and b) slightly higher magnification TEM images. c) HRTEM and d) SAED. e) Their width distribution and f) length distribution.

Metal-free CNNs are also prepared by using $[Fe(NH_3)_6]^{3+}$ as the metal complex (Figure S7). The XPS spectra of the CNNs obtained with $[Fe(NH_3)_6]^{3+}$ ions show no detectable Fe after the etching process (Figure 2b , and Figure S8). The absence of Fe in this material as well as the absence of Ru, but the presence of Pt, in the one prepared with $[Pt(NH_3)_6]^{4+}/[Ru(NH_3)_6]^{3+}$ indicate that the Fe or Ru must have been leached from the materials during etching of the silica shells. In other words, the metals with less stability under basic solutions, are leached from the CNNs during treatment under basic solutions whereas metallic Pt survived this condition.

The XPS analysis (Table S1) further reveals the presence of approximately 9 % nitrogen in the CNNs. However, the characteristic N 1s peak at around 397 eV is not observed in the XPS spectrum of the control sample prepared from CeNWs with no metal amine complexes (and presumably with no silica shells). Thus, the nitrogen detected on the CNNs must have come from the thermal decomposition of the metal amine complexes. This result also demonstrates the ability of the silica shells to keep not only carbon

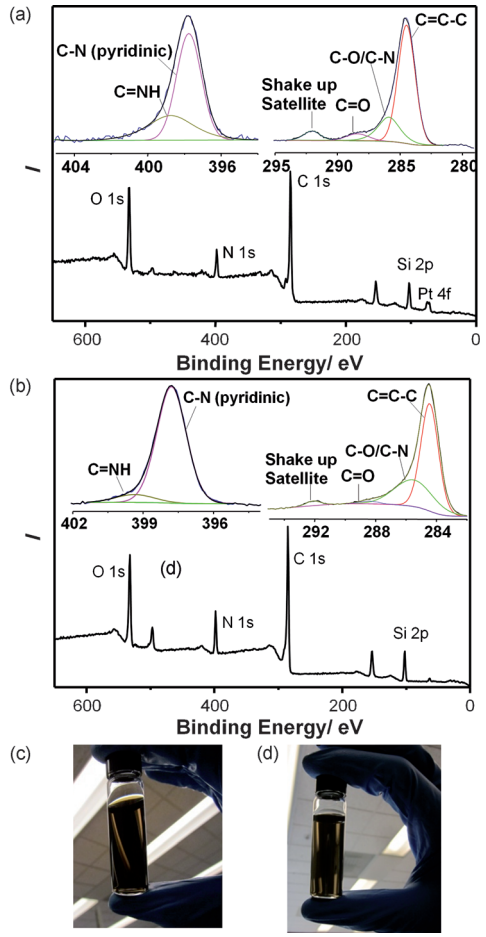

Figure 2. XPS spectra of CNNs obtained from a) CeNW/$[Pt(NH_3)_6]^{4+}$/$[Ru(NH_3)_6]^{3}$/silica after etching of the silica shells, and b) CeNW/$[Fe(NH_3)_6]^{3+}$/silica after etching of the silica shells. Digital photographs of aqueous solutions of CNNs after etching of the silica shells, showing highly dispersed carbon nanomaterials, obtained from c) CeNW/$[Pt(NH_3)_6]^{4+}$/$[Ru(NH_3)_6]^{3}$/silica, and d) CeNW/$[Fe(NH_3)_6]^{3+}$/silica.

but also nitrogen species from escaping from the inner cores of the CeNWs/metal complex/silica core–shell–shell nanoreactors during thermal treatments.

By deconvolution of the N 1s signal at approximately 397.8 eV in the XPS spectrum, the nitrogen atoms in the resulting CNNs are determined to be predominantly pyridinic nitrogen atoms.[20] The presence of such high percentage of nitrogen species in the CNNs must have also been why the CNNs are highly dispersible and stable in aqueous solutions (Figures 2c and d). In addition, the O1s peak at around 532 eV in the XPS spectra is observed. This peak is mainly attributed to possible silica residues on the material. A strong shake-up satellite band at approximately 292 eV in the XPS spectra is assigned to the π to π* transitions of the C=C bonds in the CNNs. This band normally appears less intense and broader for aromatic materials.[21] Thus, its relatively high intensity in the XPS spectra of CNNs is indicative of the presence of high cross-section of delocalized π*-orbital electrons on the carbon atoms of the CNN materials.

The micro-Raman spectra of CNNs show the typical D and G bands at around 1350 and 1602 cm^{-1}, respectively, and a less intense 2D band at approximately 2700 cm^{-1} (Figure 3a). The position of the G band is remarkably upshifted compared with that of bulk graphite (ca. 1580 cm^{-1}). The upshift of the G band is often attributed to the confinement effect of phonon modes,[22] which in our case should be the result of the smaller planar sizes of the CNN crystallites. Moreover, the appearance of an intense first-order D band is often associated with structural defects in the basal planes and the edge plane in carbon nanomaterials.[23] Thus, since the TEM images and the SAED pattern indicate that the CNN materials have well-organized structures (appear highly crystalline), we attribute the observed intense D band as well as its associated overtone, 2D band, for these materials to their small crystallite sizes and the presence of high proportions of edge planes in their structures.

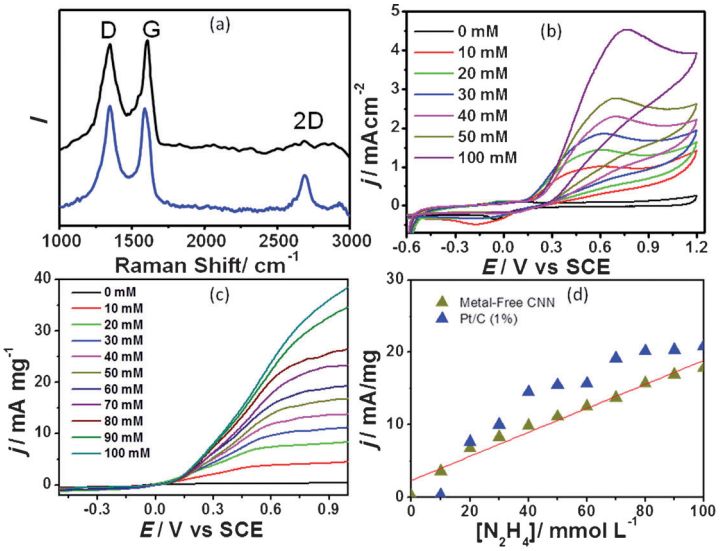

Figure 3. Raman spectra, and electrochemical and electrocatalytic properties of CNNs. a) Raman spectra of CNNs obtained with $[Pt(NH_3)_6]^{4+}$/$[Ru(NH_3)_6]^{3+}$ (blue) and $[Fe(NH_3)_6]^{3+}$ (black). b) Cyclic voltammetry at 20 $mV s^{-1}$ of CNNs, prepared from CeNW/$[Fe(NH_3)_6]^{3+}$/silica at pH 7.4 in 0.1 M PBS using different concentrations of hydrazine. c) Polarization curve (800 rpm and 20 $mV s^{-1}$) for CNN sample prepared using $[Fe(NH_3)_6]^{3+}$ ions and different concentrations of hydrazine solution. d) Mass activity at constant potential (0.5 V) in function of hydrazine concentration obtained from the polarization curve for metal-free CNNs and Pt/C (1% Pt content).

By using the CNNs obtained from CeNW/metal complex/silica core–shell–shell nanoneedles prepared with $[Fe(NH_3)_6]^{3+}$ as electrocatalysts, the catalytic oxidation of hydrazine was performed. Since hydrazine is regarded as a potential fuel in fuels cells,[24] successful electrocatalytic oxidation of hydrazine, especially without using conventional Pt-based catalysts, may have far-reaching implications.[25,26] The cyclic voltammetry (CV) response of these metal-free CNNs toward electrocatalytic hydrazine oxidation (at pH 7.4 in 0.1 M phosphate-buffer-saline, PBS solution) shows a strong anodic peak starting at approximately 0.15 V versus saturated

calomel electrode (SCE) for 10 mM hydrazine solution (Figure 3b). As this peak is associated with the oxidation of hydrazine, the result indicates the efficient electrooxidative catalytic activity of CNNs (Table S3). This result is further verified by polarization measurements of CNNs in different concentration of hydrazine (Figure 3c). From the polarization curves, a linear relationship between current and hydrazine concentration at a constant potential of 0.5 V is obtained (Figure 3d). The CNNs give a mass activity of approximately 18 mA mg^{-1} CNNs for 100 mmol L^{-1} of hydrazine solution at 0.5 V. This result clearly reveals that CNNs can be successfully used as efficient electrocatalysts for hydrazine oxidation. The origin of the CNNs' high catalytic activity is most likely their unique structures and large proportions of exposed edge planes (see below).

Despite being undetectable in our XPS experiment, the possible presence of trace Fe in the CNNs and its participation as catalyst in the electrocatalytic activity cannot be fully ruled out though.[27,28] Two more control experiments were, therefore, performed to evaluate the possible involvement of Fe species in the electrooxidative catalytic activity of CNNs. In the first case, the CNNs were treated with a 0.1 mol L^{-1} Fe^{3+} to increase the amount Fe species in the sample. In the second case, the CNNs were treated with 1 mol L^{-1} nitric acid to dissolve or remove any accessible Fe impurities on the materials. When Fe^{3+} is added into the material, the catalytic activity is found to be slightly lower than that of the original CNN material (Figure S13). The catalytic activity of the HNO_3-treated CNNs remains almost the same. The slightly higher overall current density (Figure S8), was mainly because of the new oxidation signal starting at −0.35 V due to the sample's treatment with HNO_3 and not because of possible changes in Fe concentration. Consequently, although Fe impurities are previously implicated to improve oxidative catalysis,[27,28] the major contribution to the activity toward the hydrazine oxidation in our case could thus be attributed only or mainly to the unique structure of the CNNs and their relatively high proportions of edge planes and N dopants.

Experimental Section

Synthesis of CeNWs: Commercially obtained cotton (6 g) was soaked in 1M aqueous NaOH solution (300 mL) for 1 h. The cotton was then removed from the solution and washed with copious amount of distilled water and dried in oven at 60 °C for 6 h. Two grams of the material was hydrolyzed in sulfuric acid solution (65 %) (80 mL) at 72 °C for 30 min under magnetic stirring (800 rpm).[9,10] The resulting solution was centrifuged at 2236 × *g* for 5 min. The supernatant was decanted and the precipitate was re-dispersed in distilled water. The solution was centrifuged again at 2236 × *g* and the resulting clear supernatant was decanted. The precipitate was dispersed again in fresh distilled water, centrifuged, and the supernatant discarded. This process was repeated until the supernatant remained opaque even after centrifugation as a result of the better dispersion of the well-washed CeNWs. At this point, the supernatant as well as the residual precipitate were sonicated for 6 h. The dispersion was centrifuged again at 2236 × *g* for 5 min. The supernatant was separated and further centrifuged for 15 min at 9659 × *g*, resulting in CeNWs as precipitate.

Synthesis of carbon nanoneedles (CNNs): Two solutions, each containing CeNWs (500 mg), water (24 mL) and absolute ethanol (200 mL), were prepared. To the first solution, $FeCl_3$ (0.1 mmol) was added. To the second solution, $RuCl_3 \cdot 3H_2O$ (0.05 mmol) and $H_2PtCl_6 \cdot 6H_2O$ (0.05 mmol) were added. Both solutions were stirred for 30 min. After adding ammonia solution (5 mL; 25 %) to each of them, they were stirred for another 30 min. Then tetraethyl orthosilicate (1 mL) was added into each solution. The solutions were sonicated in an ultrasonic bath for 1 h and then stirred for another 12 h with a magnetic stirrer. The precipitate was recovered by centrifugation and the supernatant was decanted. The precipitate was washed repeatedly with ethanol under sonication, followed by centrifugation and decantation. The precipitate was then dried and crushed in a mortar and pestle. The resulting powder was thermally treated in nitrogen atmosphere as indicated in Information Figure S2. The silica shell was removed by stirring 50 mg of the powder material in aqueous NaOH solution (50 mL; 2M) for 72 h. A dark powdered material consisting of carbon nanoneedles (CNNs) was recovered by centrifugation of the solution at 18514x*g* for 30 min and washing it three times with ethanol under sonication, followed by centrifugation and decantation.

Received: March 3, 2012
Revised: April 30, 2012
Published online: June 8, 2012

Keywords: carbon nanoneedles · electrocatalysis · fuel cells · metal-free catalysis · nitrogen-doped nanomaterials

[1] J. Cao, Q. Wang, H. Dai, *Nat. Mater.* **2005**, *4*, 745 – 749.
[2] S. Iijima, C. Brabec, A. Maiti, J. Bernholc, *J. Chem. Phys.* **1996**, *104*, 2089.
[3] C. Berger, Z. Song, T. Li, X. Li, A. Y. Ogbazghi, R. Feng, Z. Dai, A. N. Marchenkov, E. H. Conrad, P. N. First, W. A. de Heer, *J. Phys. Chem. B* **2004**, *108*, 19912 – 19916.
[4] A. Hirsch, *Nat. Mater.* **2010**, *9*, 868 – 871.
[5] P. J. Britto, K. S. V. Santhanam, P. M. Ajayan, *Bioelectrochem. Bioenerg.* **1996**, *41*, 121 – 125.
[6] C. E. Banks, T. J. Davies, G. G. Wildgoose, R. G. Compton, *Chem. Commun.* **2005**, 829 – 841.
[7] R. R. Moore, C. E. Banks, R. G. Compton, *Anal. Chem.* **2004**, *76*, 2677 – 2682.
[8] C. E. Banks, R. G. Compton, *Analyst* **2006**, *131*, 15 – 21.
[9] M. Sevilla, C. Sanchís, T. Valdés-Solís, E. Morallón, A. B. Fuertes, *Carbon* **2008**, *46*, 931 – 939.
[10] M. Sevilla, A. B. Fuertes, *Chem. Phys. Lett.* **2010**, *490*, 63 – 68.
[11] K. E. Shopsowitz, H. Qi, W. Y. Hamad, M. J. MacLachlan, *Nature* **2010**, *468*, 422 – 425.
[12] K. E. Shopsowitz, W. Y. Hamad, M. J. MacLachlan, *Angew. Chem.* **2011**, *123*, 11183 – 11187; *Angew. Chem. Int. Ed.* **2011**, *50*, 10991 – 10995.
[13] Y. Habibi, L. A. Lucia, O. J. Rojas, *Chem. Rev.* **2010**, *110*, 3479 – 3500.
[14] S. Elazzouzi-Hafraoui, Y. Nishiyama, J.-L. Putaux, L. Heux, F. Dubreuil, C. Rochas, *Biomacromolecules* **2008**, *9*, 57 – 65.
[15] E. D. Cranston, D. G. Gray, *Sci. Technol. Adv. Mater.* **2006**, *7*, 319 – 321.
[16] F. J. Maldonado-Hódar, C. M. Castilla, J. R. Utrilla, Y. Hanzawa, Y. Yamada, *Langmuir* **2000**, *16*, 4367 – 4373.
[17] J. R. Matos, M. Kruk, L. P. Mercuri, M. Jaroniec, L. Zhao, T. Kamiyama, O. Terasaki, T. J. Pinnavaia, Y. Liu, *J. Am. Chem. Soc.* **2003**, *125*, 821 – 829.
[18] Z. Czigány, L. Hultman, *Ultramicroscopy* **2010**, *110*, 815 – 819.
[19] N. Isomura, X. Wu, H. Hirata, Y. Watanabe, *J. Vac. Sci. Technol. A* **2010**, *28*, 1141 – 1144.
[20] A. Bagreev, G. Nanse, J. Lahaye, V. Strelko, *Carbon* **1999**, *37*, 585 – 590.
[21] B. Gao, Z. Y. Wu, Y. Luo, *J. Chem. Phys.* **2008**, *128*, 234704.

[22] P. Tan, S. Dimovski, Y. Gogotsi, *Philos. Trans. R. Soc. London Ser. A* **2004**, *362*, 2289 – 2297.
[23] Q. Yu, Q. Yu, L. A. Jauregui, W. Wu, R. Colby, J. Tian, Z. Su, H. Cao, Z. Liu, D. Pandey, D. Wei, T. F. Chung, P. Peng, N. P. Guisinger, E. A. Stach, J. Bao, S.-S. Pei, Y. P. Chen, *Nat. Mater.* **2011**, *10*, 443 – 449.
[24] A. Serov, C. Kwak, *Appl. Catal. B* **2010**, *98*, 1 – 9.
[25] J. Sanabria-Chinchilla, K. Asazawa, T. Sakamoto, K. Yamada, H. Tanaka, P. Strasser, *J. Am. Chem. Soc.* **2011**, *133*, 5425 – 5431.
[26] R. Silva, T. Asefa, *Adv. Mater.* **2012**, *24*, 1878 – 1883.
[27] C. E. Banks, A. Crossley, C. Salter, S. J. Wilkins, R. G. Compton, *Angew. Chem.* **2006**, *118*, 2595 – 2599; *Angew. Chem. Int. Ed.* **2006**, *45*, 2533 – 2537.
[28] G. Wu, K. L. More, C. M. Johnston, P. Zelenay, *Science* **2011**, *332*, 443 – 447.

